# Competing fracture modes in brittle materials subject to concentrated cyclic loading in liquid environments: Bilayer structures

Sanjit Bhowmick
*Materials Science and Engineering Laboratory, National Institute of Standards and Technology, Gaithersburg, Maryland 20899-8500*

Yu Zhang
*New York University College of Dentistry, New York, New York 10010*

Brian R. Lawn[a)]
*Materials Science and Engineering Laboratory, National Institute of Standards and Technology, Gaithersburg, Maryland 20899-8500*

(Received 18 April 2005; accepted 7 July 2005)

A preceding study of the competition between fracture modes in monolithic brittle materials in cyclic loading with curved indenters in liquid environments is here extended to brittle layers on compliant substrates. The fracture modes include outer and inner cone cracks and radial cracks that initiate from the near-contact zone and penetrate downward. Outer cone cracks are driven by stresses from superposed Hertzian and plate flexure fields; inner cone cracks also grow within these fields but are augmented by mechanical driving forces from hydraulic pumping into the crack fissures. Radial cracks are augmented by mechanical driving forces from developing quasiplasticity zones beneath the indenter. Basically, the crack-growth rates are governed by a crack velocity relation. However, the hydraulic and quasiplastic mechanical forces can cumulate in intensity with each cycle, strongly enhancing fatigue. Plate flexure generates compressive stresses at the top surface of the brittle layer, somewhat inhibiting the initiation, and tensile stresses at the lower surface, strongly enhancing the far-field propagation. The tensile stresses promote instability in the crack propagation, resulting in through-thickness penetration (failure). Experiments on a model bilayer system consisting of glass plates bonded to thick polycarbonate bases are presented as an illustrative case study. In situ observations of the crack evolution from initial growth to failure reveal that each fracture mode can dominate under certain test conditions, depending on plate thickness, maximum load, and sphere radius. Implications concerning the failure of practical layer systems, notably dental crowns, are discussed.

## I. INTRODUCTION

This paper follows on from a preceding study of the competition between various fracture modes in monolithic brittle solids subjected to cyclic contact with curved indenters in liquids.[1] Consideration was there given to three crack types that initiate within the near-contact field, depicted in Fig. 1: outer cone cracks (**O**), which form outside the maximum contact and are driven downward and outward solely by Hertzian stresses; inner cone cracks (**I**), which form inside the maximum contact and penetrate more steeply downward, driven also by Hertzian stresses but augmented by internal hydraulic pumping stresses from entrapped fluid within the confining crack walls (exacerbated by crack mouth closure at the indenter contact); and radial cracks (**R**), which generate from within a quasiplastic zone of shear-activated microdamage immediately beneath the contact and extend directly downward on median planes containing the load axis. We extend that previous study here to include the case of brittle layers of finite thickness bonded to lower-modulus support bases. Such layer systems are relevant to a wide variety of engineering and biomechanical structures,[2] of which we regard dental crowns on tooth dentin as archetypal. The main difference between layer structures and their monolith counterparts is

[a)]Address all correspondence to this author.
e-mail: brian.lawn@nist.gov
DOI: 10.1557/JMR.2005.0335

 

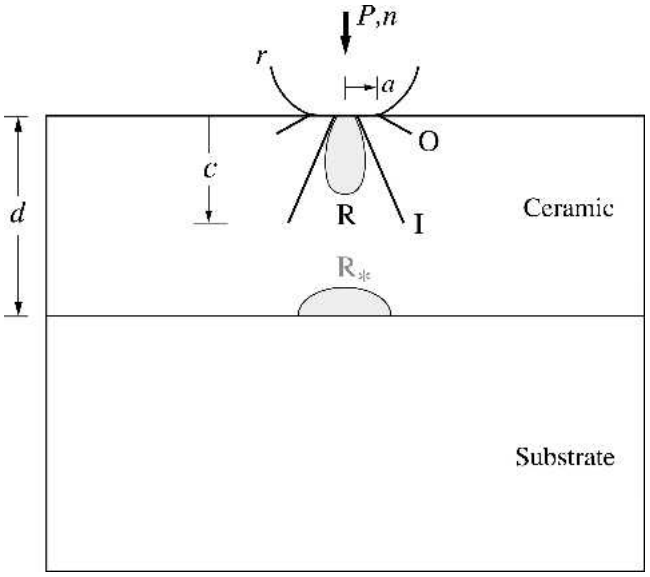


FIG. 1. Schematic illustration of crack geometry for cyclic contact on brittle layer bonded to compliant support bases with sphere of radius $r$ at load $P$ and contact radius $a$ for number of cycles $n$. Top-surface crack modes, through-thickness size $c$ are shown: outer cone cracks (**O**), inner cone cracks (**I**), and radial cracks (**R**). Another kind of radial crack ($\mathbf{R}_*$) can occur at the bottom surface but is neglected in this study.

the superposition of stresses arising from flexure of the brittle plate on the compliant support, so that deeper penetrating cracks experience increasing tension in the depth of the plate and ultimately cause through-thickness failure. Cyclic loading of the contact generally accelerates downward extension of the cracks into the subsurface region, basically by slow crack growth from chemical interaction with environmental water but also from cumulative mechanical driving forces: in the case of **I** cracks, by hydraulic pumping from intrusive liquid;[3] and in the case of **R** cracks, from residual stresses within a precursor quasiplasticity zone.[4]

Accordingly, in this paper the competition between fracture modes in brittle layers on compliant substrates under cyclic loading with curved indenters in liquid environment is examined. Soda-lime glass is retained as our model test material, but in this case is prepared as plates 2.2 mm and 1 mm thick bonded onto thick polycarbonate bases using epoxy adhesive, as described in previous studies.[5] Cyclic indentation tests are made on the glass surfaces using tungsten carbide spheres in water. Our choice of glass plate thicknesses represents a compromise: thick enough that the only cracks are those formed at the top surface, yet thin enough that plate flexural stresses play a significant role in the fracture evolution. In thinner plates, typically < 1 mm, a second kind of radial crack can initiate at the bottom surface ($\mathbf{R}_*$ in Fig. 1). This last crack type has been well documented elsewhere and will not be considered in any detail here.[5–7] In our tests, the entire crack evolution within the glass layers is followed in situ, from first sighting to ultimate penetration to the interface. We show that each crack mode can cause failure under certain conditions, depending on plate thickness, maximum load, and sphere radius. **I** and **R** cracks, although relatively sluggish in their initiation, are especially dangerous under prolonged cycling, overtaking their **O** crack predecessors and accelerating rapidly in the later stages of growth. A generic fracture mechanics analysis provides an approximate basis for understanding the role of key test variables in the ultimate failure condition.

## II. EXPERIMENTAL

A specimen preparation procedure similar to that used in previous studies was adopted here.[5,8] Soda-lime glass plates 2.2 and 1 mm thick and 50 × 25 mm lateral dimensions were polished at their edges to enable side viewing during testing. The top surfaces of the plates were pre-abraded with grade 600 SiC grit to produce a uniform layer of starting surface flaws for cone cracks, and the bottom surfaces pre-etched with HF to minimize intrusion of lower interface radial ($\mathbf{R}_*$) cracks. The plates were then bonded to polycarbonate slabs 12.5 mm thick using epoxy glue. Some monolithic glass slabs were retained as a reference baseline for comparison.

As in the preceding study,[1] contact testing was effected by loading the top surfaces with WC spheres of fixed sphere radius $r = 1.58$ mm over $n$ cycles at a frequency $f = 1$ Hz. Some additional tests were run with larger spheres, $r = 5.15$ mm. Maximum loads ranged from $P_m = 75$ up to 750 N, with a minimum "hold" load 2 N to prevent the indenter from "wandering" over the specimen surfaces. A drop of water placed in the contact zone was continually replenished during the tests. A video camera system was placed to view the crack evolution from the side, with a slight upward tilt so the subsurface contact could be observed. Crack depths $c$ for each fracture mode were recorded at the deepest points, as a function of $n$. Generally, the outer (**O**) cone cracks appeared first, within the first cycle at nearly all loads. As previously, some difficulty was experienced in observing the initial stages of the top-surface inner (**I**) cone and radial (**R**) cracks, but the ensuing propagation stages were clearer once these cracks penetrated below the **O** base rim. In all tests, the cycling was stopped once failure occurred.

## III. RESULTS

### A. Crack morphology

The evolution characteristics of all crack types for the glass plates on polycarbonate support bases were similar

to those for monoliths in the initial stages but notably different in the ensuing propagation stages. Most striking was the tendency for the cracks to instability and rapid failure on approaching the midpoint of the glass layer after a critical number of cycles $n_F$. Examples of failure from each crack mode are shown in Fig. 2 for glass thickness $d = 2.2$ mm and sphere radius $r = 1.58$ mm: (a) **O** crack (load $P_m = 600$ N), (b) **I** crack ($P_m = 500$ N), and (c) **R** crack ($P_m = 400$ N). In all cases illustrated, an **O** crack formed in the first cycle, in (a) propagating to failure before any of its rivals appeared, while in (b) and (c), it was overtaken by its **I** crack and **R** crack rivals after extended cycling. There was no indication of any delamination at the glass/epoxy or epoxy/polycarbonate interfaces prior to full penetration of any crack, attesting to the bond strength in these specimens. Where failure was uncommonly catastrophic, usually at higher loads, some glass plates separated from the polycarbonate bases. In the case of **R** failures, the crack usually penetrated by elongating into a narrow kidney shape toward the glass/polycarbonate interface, followed by an upward and outward expansion into the near-elliptical form of classical bottom-surface $\mathbf{R}_*$ cracks. The beginnings of this latter phase in the evolution is evident as the dark "wings" in Fig. 2(c).

There was evidence of interactions between competing cracks in the later stages of evolution. Once any crack begins to penetrate into the lower depths, it increases the plate compliance, making it easier for competitors to extend. Failure from any one crack type was often succeeded quickly by instability of the others. Such

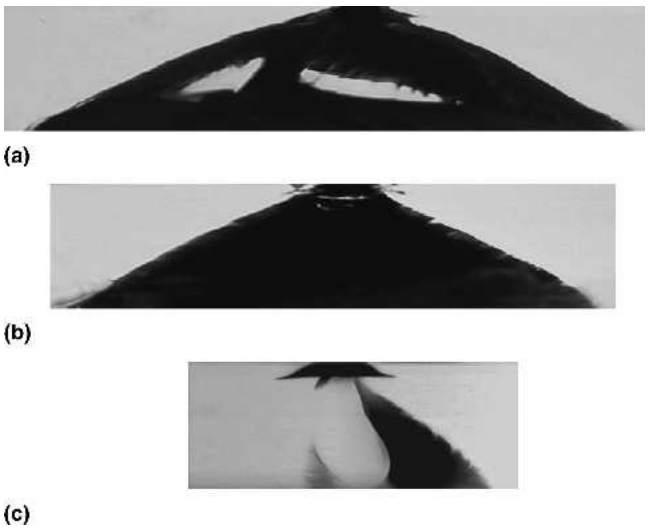


FIG. 2. Side views of failures of Hertzian indentation sites in soda-lime glass plates of thickness $d = 2.2$ mm during cycling at 1 Hz in water with WC spheres of radius $r = 1.58$ mm and frequency 1 Hz. (a) Outer **O** cone crack at $P_m = 600$ N after $n_F = 1.4 \times 10^3$ cycles, (b) inner **I** cone crack at $P_m = 500$ N after $n_F = 228$ cycles, and (c) median–radial **R** crack at $P_m = 400$ N after $n_F = 5 \times 10^3$ cycles. In all three cases, the dominant crack has penetrated the glass layer.

complex behavior would make post-mortem fractographic analysis extremely difficult, potentially leading to false conclusions.

### B. Crack evolution

Figure 3 plots crack depth $c$ as function of number of cycles $n$ for three thicknesses $d$ of glass layer for cyclic loading with a sphere of radius $r = 1.58$ mm at common maximum load $P_m = 200$ N, in water: (a) $d = \infty$ (monolith), (b) $d = 2.2$ mm, and (c) $d = 1$ mm. Each test is indicated by a different symbol. The load is such that an **O** crack forms during the first cycle in each configuration. In the monolith [Fig. 3(a)], the **O** crack is overtaken by **I** cracks at $n \approx 10^3$ cycles in two tests, and by **R** cracks at $n \approx 10^4$ cycles in a third test. In this specimen, all cracks tend to a steady state plateau at large $n$.[1] For the intermediate plate [Fig. 3(b)], through-thickness failure occurs in one test from an **I** crack and in another from an **R** crack, between $n = 10^5$ and $10^6$ cycles. For the thin plate [Fig. 3(c)], the **O** crack is responsible for failure in two of three tests. In these two instances failure occurs at $n \approx 3 \times 10^3$ cycles, before either **I** or **R** cracks appear. In the third test, a rival **I** crack appears and quickly becomes the source of failure. In this specimen configuration, there was little indication of a steady state in the propagation prior to failure, especially in the **I** or **R** cracks. Taken together, the data in Fig. 3 reveal a strong tendency to more rapid failure in thinner plates.

An important variable in the failure process is the maximum contact load $P_m$. Clearly, higher loads are expected to increase crack sizes and promote failure. The role of this variable is illustrated by $c(n)$ data in Figs. 4, 5, and 6 for glass plate thicknesses $d = \infty$ (monolith), $d = 2.2$ mm, and $d = 1$ mm, respectively, at common sphere radius $r = 1.58$ mm. Data are shown separately for (a) **O**, (b) **I**, and (c) **R** cracks. The data for monolithic glass plates (Fig. 4) have been previously documented[1] and are reproduced here simply for comparison with bilayers. Again, **O** cracks tend always to form first, within or shortly after the first cycle, regardless of $P_m$. At higher $P_m$ values, both **I** cracks and **R** cracks tend to catch up and grow deeper in the intermediate $n$ region. All crack types at these higher loads tend to a steady state at large $n$ in the monoliths, corresponding to a far-field dependence $c \sim n^{-2/3N}$, where $N = 17.9$ is a crack velocity exponent for glass in water (solid lines).[1] At lower $P_m$, **I** and (especially) **R** cracks tend to form well after their **O** crack predecessors, without ever achieving steady state over the cycle range.

Now consider plates of thickness $d = 2.2$ mm (Fig. 5). Because of superposition of plate flexure stresses, the cracks are accelerated in their later stages and failures can occur. At higher loads, $P_m > 600$ N, **O** cracks form first and usually penetrate the plate before any rivals appear. At intermediate loads, 600 N $< P_m <$ 400 N, **I**

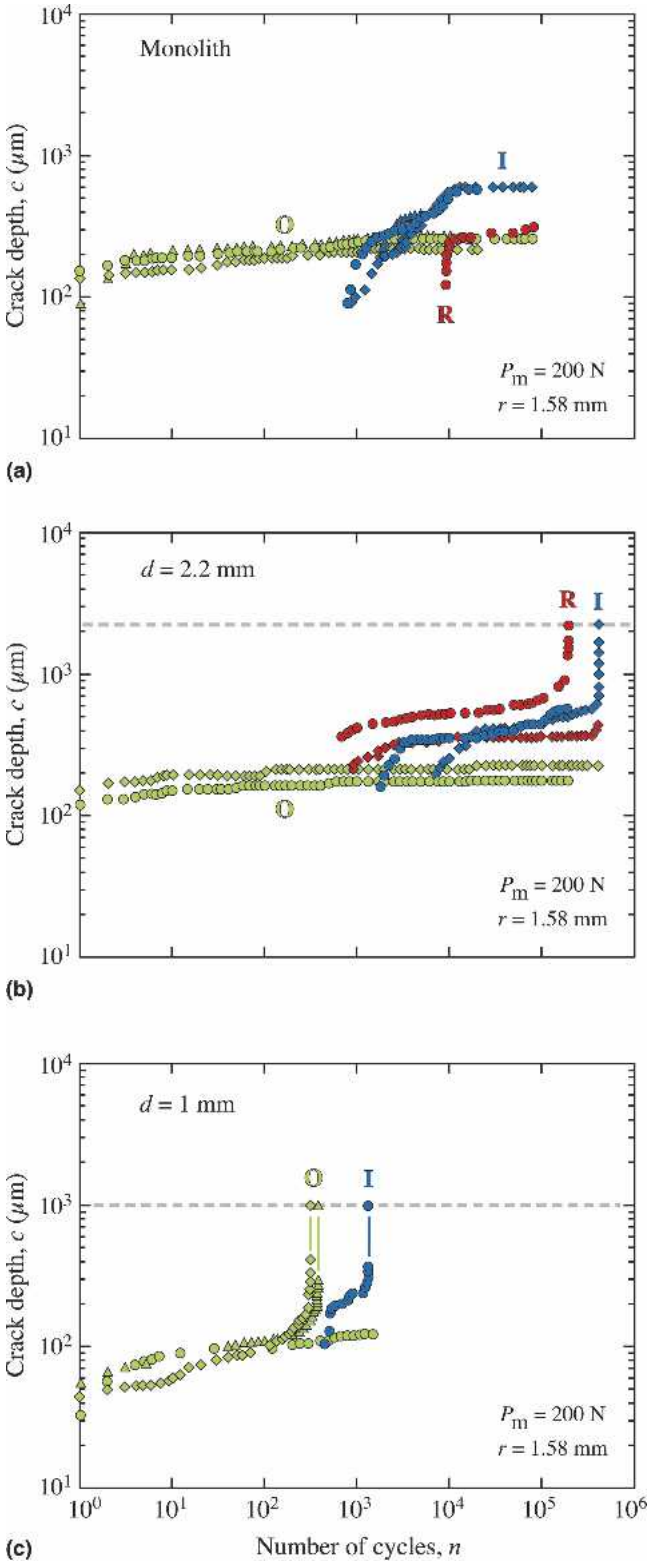


FIG. 3. Crack depth $c$ for abraded glass as function of number of cycles $n$ for indentation with WC sphere of radius $r$ = 1.58 mm, maximum load $P_m$ = 200 N, and frequency 1 Hz in water. Data for glass thicknesses $d$: (a) $d = \infty$ (monolith), (b) $d$ = 2.2 mm, and (c) $d$ = 1 mm (horizontal dashed lines). Each symbol represents a separate test. Note how **O** cracks form first but are ultimately overtaken by **I** and (especially) **R** cracks.

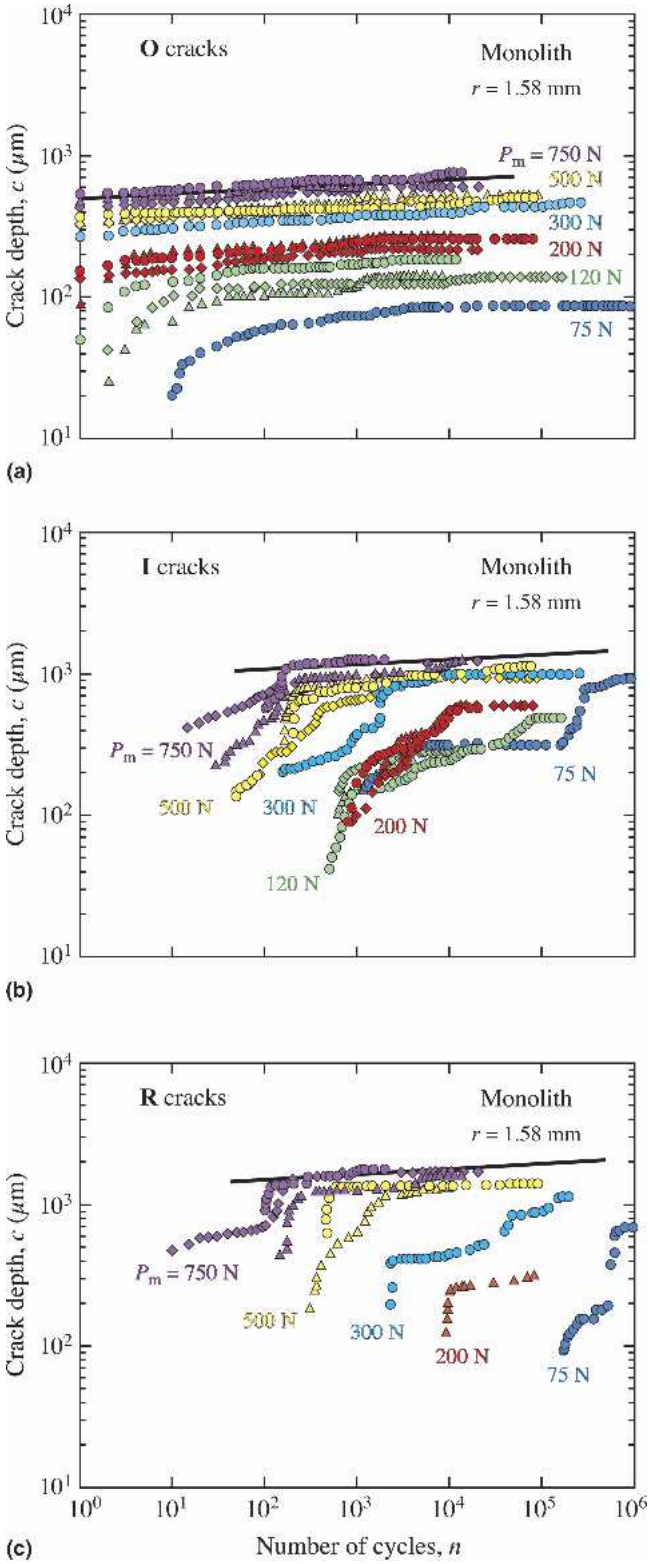


FIG. 4. Crack depth $c$ as function of number of cycles $n$ for (a) **O** cracks, (b) **I** cracks, and (c) **R** cracks in monolith soda-lime glass. Tests were performed in water with WC sphere of radius $r$ = 1.58 mm and frequency 1 Hz for specified $P_m$. Each symbol represents a separate test. Solid lines are asymptotic steady state limit for far-field cracks (shown here only for $P_m$ = 750 N). Data are reproduced from Zhang et al.[3]

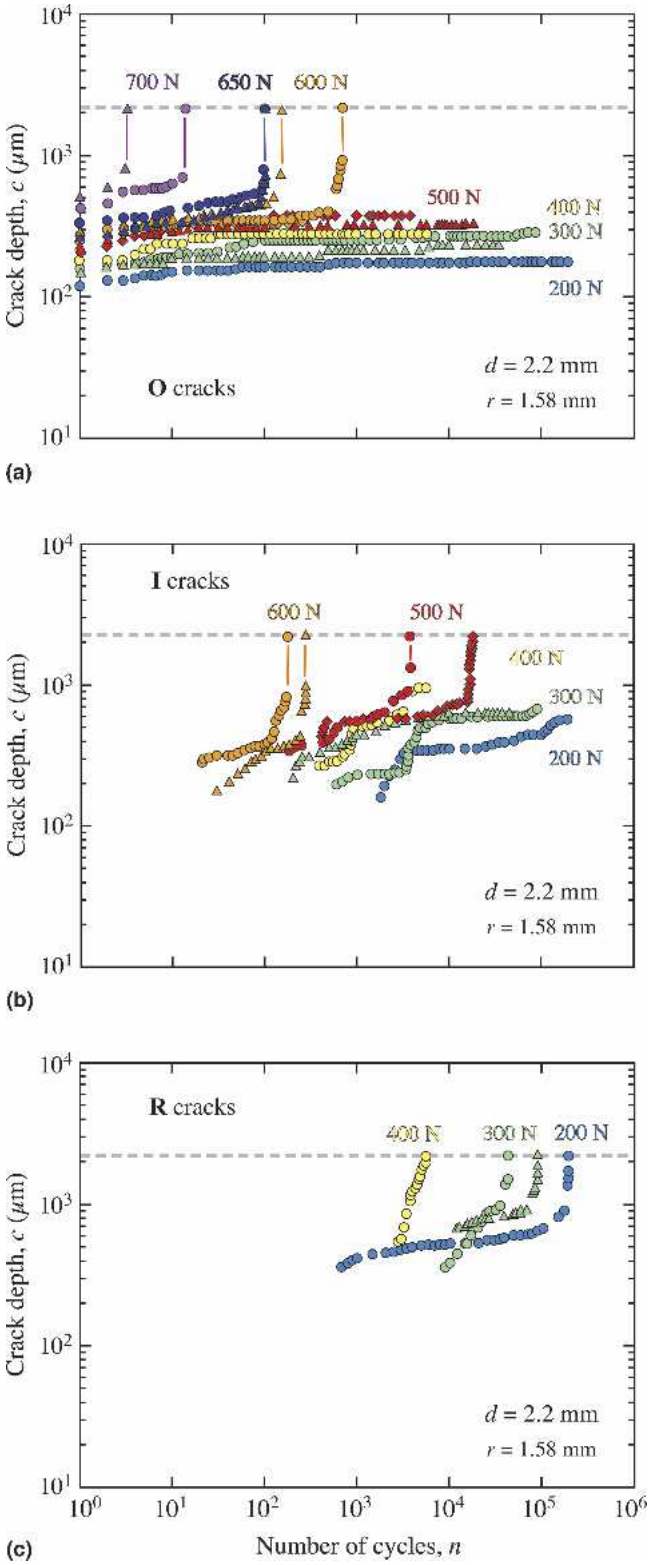


FIG. 5. Crack depth $c$ as function of number of cycles $n$ for (a) **O** cracks, (b) **I** cracks and (c) **R** cracks in soda-lime-glass/polycarbonate bilayer with glass thickness $d = 2.2$ mm (horizontal dashed lines). Tests were performed in water with WC sphere of radius $r = 1.58$ mm and frequency 1 Hz for specified $P_m$. Each symbol represents a separate test. Note failure from **O** cracks at loads $P_m > 600$ N, from **I** cracks within 600 N $> P_m >$ 400 N, and from **R** cracks at $P_m < 400$ N.

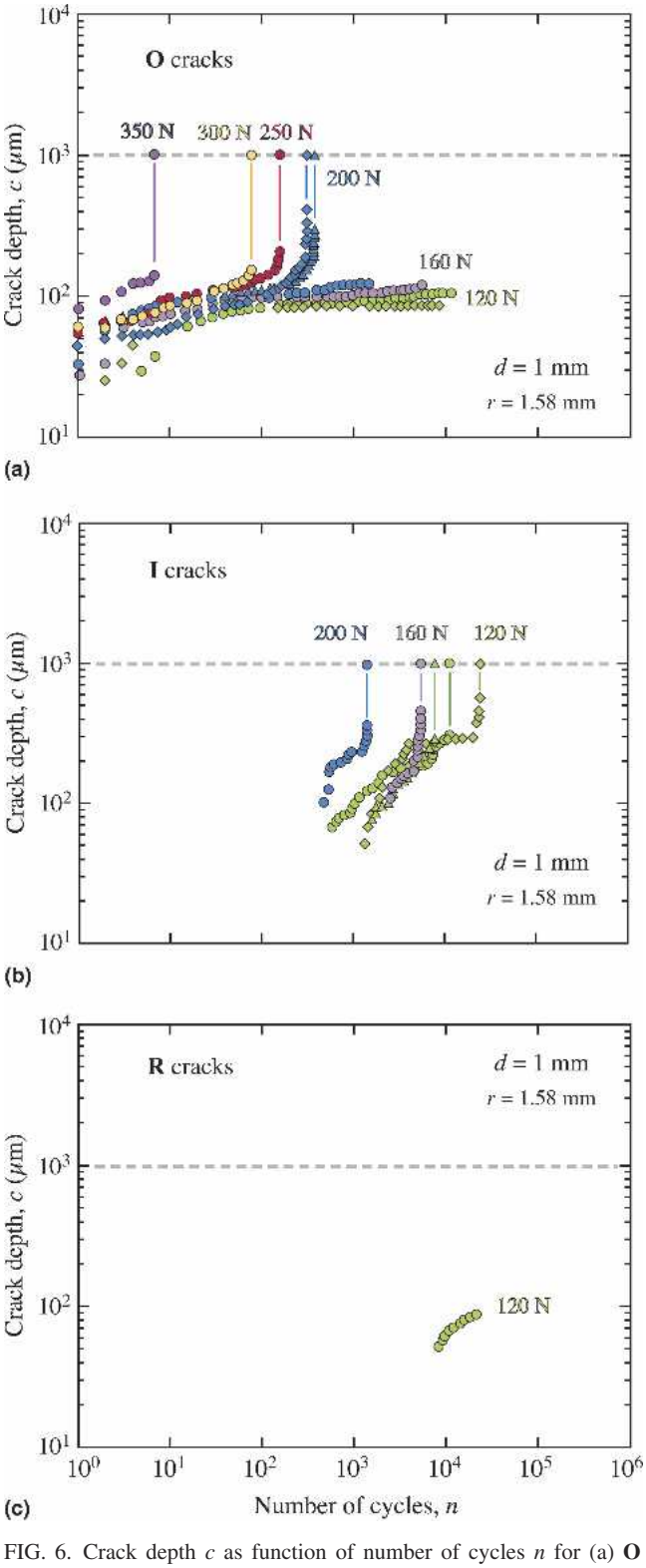


FIG. 6. Crack depth $c$ as function of number of cycles $n$ for (a) **O** cracks, (b) **I** cracks, and (c) **R** cracks in soda-lime-glass/polycarbonate bilayer with glass thickness $d = 1$ mm (horizontal dashed lines). Tests were performed in water with WC sphere of radius $r = 1.58$ mm and frequency 1 Hz for specified $P_m$. Each symbol represents a separate test. Note failure from **O** cracks at loads $P_m > 200$ N, from **I** cracks within 200 N $> P_m >$ 120 N, and absence of failure from **R** cracks over cyclic range.

cracks appear and become the dominant source of failure. At lower loads, $P_m < 400$ N, **R** cracks, although last to form, ultimately win out [Fig. 5(c)]. The competition between the crack types is most evident in tests in the load transition regions in Fig. 5: e.g., failure from either **O** or **I** cracks in separate tests at $P_m = 600$ N, and from either **I** or **R** cracks in separate tests at $P_m = 400$ N. In Fig. 5, the critical cracks, especially **I** and **R** cracks, show less tendency to steady state prior to failure than in their monolith counterparts in Fig. 4.

Even more pronounced failure characteristics are apparent in plates of thickness $d = 1$ mm (Fig. 6). In these specimens, the loads for dominance of each crack type were considerably diminished relative to the thicker specimens, i.e., $P_m > 200$ N for **O** cracks, 200 N $> P_m >$ 120 N for **I** cracks, and no failures at all for **R** cracks over the $n$ test range. Again, there is overlap in **O** and **I** failure modes in separate tests at $P_m = 200$ N. The **I** cracks show even less tendency to steady state before failure than in the thicker specimens in Fig. 5.

Another important variable is sphere radius $r$. One may expect diminished failure tendency at higher $r$ at any given load because of reduced Hertzian pressure. A plot of $c(n)$ is presented in Fig. 7 for $r = 3.18$ and 5.15 mm, at common plate thickness $d = 2.2$ mm and load $P_m = 500$ N. In this case, data are shown only for (a) **O** and (b) **I** cracks, since **R** cracks do not have a chance to form at $P_m > 400$ N under these test conditions (Fig. 5). In this instance, any shifts in data for different sphere radii appear to be obscured by the scatter.

### C. Critical conditions for bilayer failure

The most distinctive feature of the fracture evolution in the glass layer structures relative to monoliths is the tendency for the cracks to penetrate through to the lower interface and thereby cause failure. A plot of the number of cycles $n_F$ to failure is given as a function of $P_m$ in Fig. 8 for the two glass thicknesses $d = 2.2$ mm and 1 mm. Different crack modes are indicated by different symbols in this figure. **O** cracks are responsible for failure at high $P_m$, **I** cracks at intermediate $P_m$, and **R** cracks at low $P_m$. A significant shift to lower $n_F$ is evident in the thinner plates. It is clear that prolonged cycling can promote several failure modes in brittle layer systems.

A general condition for failure in brittle bilayers is beyond the scope of this study because of the superposition of Hertzian and flexure stress fields plus additional mechanical stresses from hydraulic pumping and quasiplastic degradation. These complexities are reflected in the complex $c(n)$ dependencies in Figs. 3–7. Nevertheless, a limiting relation for the critical number of cycles $n_F$ to failure at $c = d$ can be obtained in a relatively straightforward manner for very long cracks (i.e., beyond the range of hydraulic and quasiplastic driving stresses) subject to a crack velocity growth law, modifying the

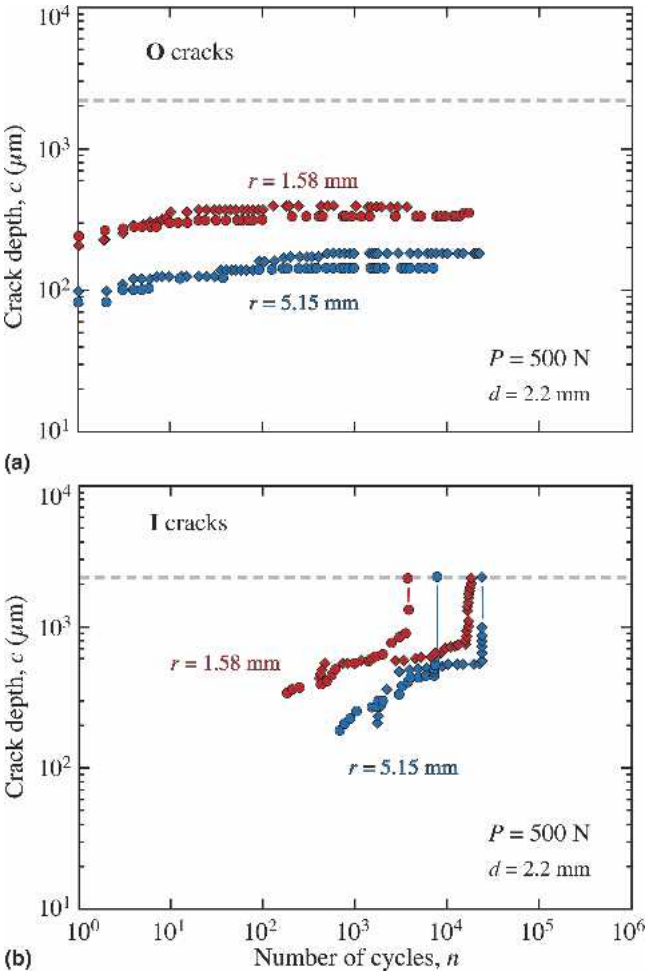


FIG. 7. Crack depth $c$ as function of number of cycles $n$ for (a) O cracks and (b) I cracks in soda-lime-glass/polycarbonate bilayer with glass thickness $d = 2.2$ mm (horizontal dashed lines) and $P_m = 500$ N (R cracks not observed at this load). Tests in water with WC sphere of radius $r = 1.58$ mm at frequency 1 Hz. Each symbol represents a separate test.

indentation stress-intensity factor to include a flexure component, as foreshadowed in the preceding study.[1] Such a relation is derived in the Appendix,

$$n_F = \gamma(fd/v_0)(Td^{3/2}/P_m)^N \quad , \qquad (1)$$

with $d$ the plate thickness, $f$ the cyclic frequency, $P_m$ the maximum contact load, $T$ the plate toughness ($K_{IC}$), $N$ and $v_0$ crack velocity parameters, and $\gamma$ a dimensionless constant. Equation (1) is indicated as the straight lines for each of the two thicknesses $d$ in Fig. 8, for $N = 17.9$. This function does not appear to represent the data very well over the full data range, especially for **I** and **R** cracks and for the thinner layers. The significant deviations at large $n$ may be ascribed at least in part to the absence of a steady state stage in the $c(n)$ data in Sec. III. B, implying that hydraulic and quasiplastic driving forces may remain active up to failure in these cases.

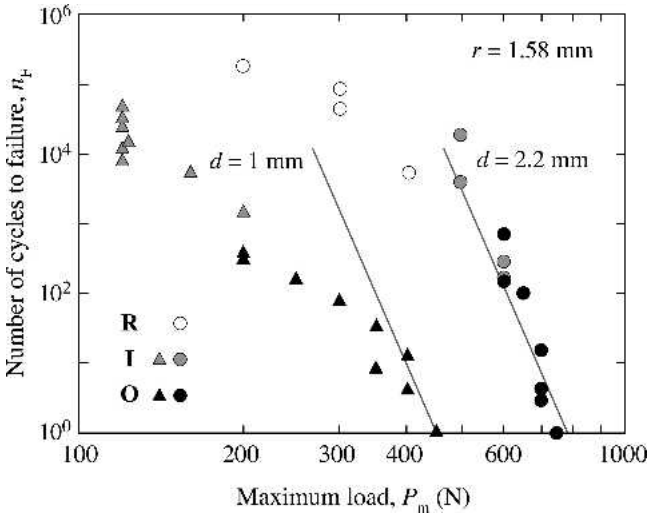


FIG. 8. Number of cycles to failure $n_F$ as function of maximum contact load $P_m$ for soda-lime-glass/polycarbonate bilayers with glass thicknesses $d = 2.2$ mm and 1 mm. Note failure from different crack modes at different $P_m$.

## IV. DISCUSSION

This paper has considered the competition between different crack types in brittle layer structures subjected to contact loading, with data on model glass/polycarbonate bilayers in water as a case study. The glass layers are sufficiently thick that the cracks form only at the top surface, yet also sufficiently thin that plate flexural stresses can accelerate the cracks rapidly through the lower section of the plate to failure. It is this tendency toward unstable failure that distinguishes the behavior of brittle bilayers from that of monoliths. Three basic crack types have been identified: outer cone cracks (**O**), which form outside the contact and are driven downward and outward by Hertzian stresses; inner cone cracks (**I**), which form inside the maximum contact and penetrate more steeply downward, augmented by internal hydraulic pumping stresses from entrapped fluid; and radial cracks (**R**), which generate from within a quasiplastic zone immediately beneath the contact and extend directly downward. Each crack mode can dominate under certain test conditions, **O** cracks at high loads $P_m$ and low number of cycles $n$, **I** cracks at intermediate $P_m$ and $n$, and **R** cracks at low $P_m$ and high $n$. Usually, in our specific material system, **O** cracks occur within the first cycle but are most often overtaken by their **I** and **R** crack rivals, as manifested by the crossovers in $c(n)$ data in Figs. 3–7. The relatively rapid surge in growth in the latter two crack modes is attributable to the cumulative nature of hydraulic pumping[3] and quasiplasticity[9] mechanisms in cyclic loading. Thus, the cracks that appear first are not necessarily those that take the system to failure.

It can be concluded that the brittle failure of systems with brittle coating layers is a complex competition between various fracture modes, specifically **O**, **I**, and **R** cracks, with considerable variability dependent on maximum contact load, layer thickness, and sphere radius, among other factors. In some cases, the competition is such that different modes may be responsible for failure in successive tests under any given set of condtions, e.g., **I** and **R** cracks in Fig. 3(b). In such instances, the competition reflects both initiation and propagation characteristics, i.e., the total evolution, determined by the simultaneous operation of hydraulic pumping and quasiplasticity driving forces in the superposed Hertzian and flexural stress fields.

We reiterate that we have not included bottom-surface-initiated radial $\mathbf{R}_*$ cracks (Fig. 1) in our current consideration. These cracks can be especially dangerous because the critical loads needed to form them fall off rapidly with diminishing thickness and because they can run easily to the specimen edges.[5–7] They will not be a factor as long as plate thickness $d$ is maintained large enough, typically $d > 1$ mm. In the context of dental crowns, it is common practice to aim for thicknesses of 1.5 mm or more; however, this aim is not easily realized due to geometrical constraints imposed by adjacent and opposing dentition. Ultimately, in optimizing material components for such systems, consideration of subsurface radial cracks will have to be factored into any complete design analysis.

Derivation of explicit fracture mechanics relations describing the general $c(n)$ crack evolution for multicycle contact loading is formidable, not only because of superposed Hertzian and flexure fields but also because of the additional hydraulic pumping and quasiplastic driving forces acting on **I** and **R** cracks, respectively.[10] Even bounding short- and long-crack cases are complex. In the short-crack region, initiation relations are especially problematic due to high stress gradients and sensitivity to assumed starting flaw conditions.[10] Nevertheless, the limited critical load expressions for onset of damage modes in monoliths presented in the preceding study[1] remain a useful first approximation for bilayers because any superposed top-surface compressive stresses from plate flexure are expected to be somewhat dominated by the Hertzian stresses in the short-crack region. In the long-crack region, the superposed tensile flexure stresses in the bottom half of the plate are expected to exert a more profound influence on the crack propagation. Accordingly, we have obtained the generic Eq. (1) for plate failure assuming a far-field stress-intensity factor—with flexural tensile stresses incorporated—in conjunction with a crack velocity law. Such assumptions imply that the cracks will have attained a steady state prior to failure. We have seen that this is not universally so in the experimental $c(n)$ data for **I** and (especially) **R** cracks. Thus while we are able to use the limited fracture mechanics relations to predict some of the broader data trends, particularly the role of key variables such as

maximum contact load $P_m$ and layer thickness $d$, a detailed analysis remains beyond the scope of this study.

Despite our incomplete theoretical understanding, we may use Eq. (1) as a basis for understanding the dependence of $n_F$ in Fig. 8 on important geometrical variables for any given sphere/bilayer combination.[11] Smaller layer thicknesses $d$ diminish $n_F$ at any given maximum load $P_m$ (Fig. 3). Lower loads $P_m$ increase $n_F$ for any given $d$ (Figs. 4–6). Blunter contacts (larger $r$) have much less effect on $n_F$ (Fig. 7). (Blunter contacts may also arise by using spheres of lower modulus, e.g., glass spheres relative to WC, as discussed in the preceding paper.[1]) Additional geometrical complications may occur in real layer systems, again exemplified by dental crowns, e.g. curvature of the layer surfaces.[12] Some recent experiments on curved specimen surfaces suggests that convexity may also reduce $n_F$. Addition of a second brittle layer to minimize flexure, e.g., stiff support core layers in dental crowns, can further alter failure characteristics.[13]

Finally, a comment on the role of material properties is in order. Our tests have been conducted on glass/polycarbonate as an ideal model bilayer system for observing crack behavior in situ. However, as emphasized in the preceding paper on monoliths, there is a certain generality for all brittle materials on compliant substrates. One issue that warrants comment here in relation to bilayers is the relative elastic modulus of the substrate. In our case, the polycarbonate base has a Young's modulus of about 3 GPa. Increasing this modulus would diminish plate flexure, reducing lower-surface tensile stresses and hence inhibiting the later stages of propagation for all crack types. In dental practice, for instance, the dentin support has a Young's modulus of 16–18 GPa. On the other hand, most dental crowns use ceramic cores with modulus several times that of glass, so the mismatch of our present system here may not be all that uncharacteristic of some important real systems.

## ACKNOWLEDGMENTS

This work was supported by a grant from the National Institute of Dental and Craniofacial Research (PO1 DE10976). Discussions with Herzl Chai and Ilja Hermann are gratefully acknowledged.

## REFERENCES

1. Y. Zhang, S. Bhowmick, and B.R. Lawn: Competing fracture modes in brittle materials subject to concentrated cyclic loading in liquid environments: Monoliths. *J. Mater. Res.* **20,** 2021 (2005).
2. B.R. Lawn, Y. Deng, P. Miranda, A. Pajares, H. Chai, and D.K. Kim: Overview: Damage in brittle layer structures from concentrated loads. *J. Mater. Res.* **17,** 3019 (2002).
3. Y. Zhang, J-K. Kwang, and B.R. Lawn: Deep penetrating conical cracks in brittle layers from hydraulic cyclic contact. *J. Biomed. Mater. Res. B* **73B,** 186 (2005).
4. D.K. Kim, Y-G. Jung, I.M. Peterson, and B.R. Lawn: Cyclic fatigue of intrinsically brittle ceramics in contact with spheres. *Acta Mater.* **47,** 4711 (1999).
5. H. Chai, B.R. Lawn, and S. Wuttiphan: Fracture modes in brittle coatings with large interlayer modulus mismatch. *J. Mater. Res.* **14,** 3805 (1999).
6. Y-W. Rhee, H-W. Kim, Y. Deng, and B.R. Lawn: Contact-induced damage in ceramic coatings on compliant substrates: Fracture mechanics and design. *J. Am. Ceram. Soc.* **84,** 1066 (2001).
7. Y. Deng, B.R. Lawn, and I.K. Lloyd: Characterization of damage modes in dental ceramic bilayer structures. *J. Biomed. Mater. Res.* **63B,** 137 (2002).
8. B.R. Lawn, Y. Deng, and V.P. Thompson: Use of contact testing in the characterization and design of all-ceramic crown-like layer structures: A review. *J. Prosthet. Dent.* **86,** 495 (2001).
9. B.R. Lawn, S.K. Lee, I.M. Peterson, and S. Wuttiphan: Model of strength degradation from Hertzian contact damage in tough ceramics. *J. Am. Ceram. Soc.* **81,** 1509 (1998).
10. H. Chai and B.R. Lawn: Hydraulically pumped cone fractures in brittle solids. (in press).
11. B.R. Lawn, K.S. Lee, H. Chai, A. Pajares, D.K. Kim, S. Wuttiphan, I.M. Peterson, and X. Hu: Damage-resistant brittle coatings. *Adv. Eng. Mater.* **2,** 745 (2000).
12. T. Qasim, M.B. Bush, X. Hu and B.R. Lawn: Contact damage in brittle coating layers: Influence of surface curvature. *J. Biomed. Mater. Res.* **73B** 179, (2005).
13. Y. Deng, P. Miranda, A. Pajares, and B.R. Lawn: Fracture of ceramic/ceramic/polymer trilayers for biomechanical applications. *J. Biomed. Mater. Res.* **67A,** 828 (2003).
14. S. Timoshenko and S. Woinowsky-Krieger: *Theory of Plates and Shells* (McGraw-Hill, New York, 1959).
15. S.M. Wiederhorn and L.H. Bolz: Stress corrosion and static fatigue of glass. *J. Am. Ceram. Soc.* **53,** 543 (1970).
16. S.M. Wiederhorn: A chemical interpretation of static fatigue. *J. Am. Ceram. Soc.* **55,** 81 (1972).

## APPENDIX: FAILURE OF FAR-FIELD CRACKS

Consider the growth of cracks initiated in the near-contact region near the top surface (Fig. A1) as they penetrate through the thickness of the ceramic plate. The

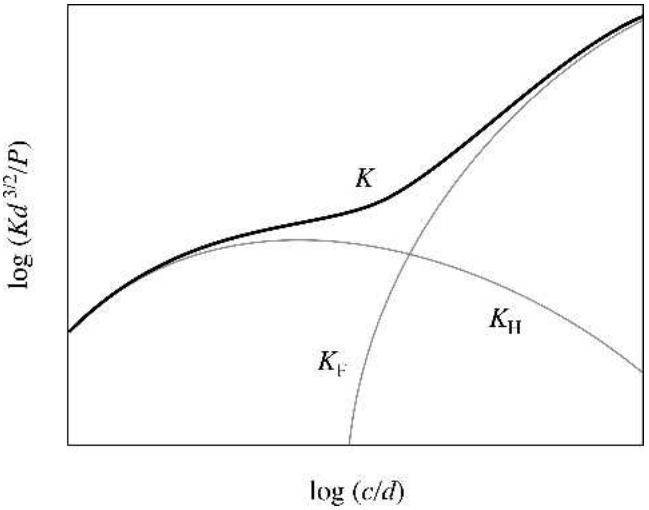


FIG. A1. Schematic plot of stress-intensity function $K = K_H + K_F$ as function of crack size $c$ (normalized and in logarithmic coordinates).

first step to determining a failure condition for these cracks is to write down a stress-intensity factor $K(P,C)$, incorporating a component from flexure of a plate (modulus $E_c$) on substrate (modulus $E_s$). The Hertzian contact component has the familiar far-field form[1]

$$K_H = \chi P/c^{3/2} \quad , \tag{A1}$$

where $\chi$ is a dimensionless crack-geometry term. The flexural component may be assumed to have the functional form[6,14]

$$K_F = \sigma c^{1/2}\, Y(c/d) \quad , \tag{A2}$$

where $\sigma = (P/Bd^2)\log(E_c/E_s)$ is the maximum flexure stress at the bottom surface of the plate, with $B$ a dimensionless constant. To bring in the contact load and plate thickness, we can write Eq. (A2) in the form

$$K_F = \psi P/d^{3/2} \quad , \tag{A3}$$

where $\psi = \psi(c/d) = (c/d)^{1/2} Y(c/d)(1/B)\log(E_c/E_s)$.

Now suppose that these two components can be superposed, $K = K_H + K_F$. Strictly this is not the case, because the terms will generally be interactive. However, such a superposition greatly simplifies the calculation. In this approximation

$$K = \chi P/c^{3/2} + \psi P/d^{3/2} = (P/d^{3/2})\, G(c/d) \quad , \tag{A4}$$

where $G(c/d) = \chi(d/c)^{3/2} + \psi(c/d)$. It is implicit in this formulation that any contributions from mechanical driving forces, hydraulic pumping and quasiplasticity, have exhausted themselves by the time the crack reaches the far field. A schematic representation of $K(c)$ is shown in Fig. A1. Whereas the $K_H$ curve has a maximum,[5] the $K_F$ curve rises steeply, resulting more or less in a monotonically increasing $K(c)$ function. Instability and failure will then occur when the crack reaches a critical depth, $c = c_*$ say, corresponding to $K > T$ ($T$ = toughness, $K_{IC}$).

To bring in rate effects, let the cracks be subject to growth according to a velocity equation[15,16]

$$\upsilon = \upsilon_0 (K/T)^N \quad , \tag{A5}$$

where $N$ is an exponent (17.9 for soda-lime glass in water[4]) and $\upsilon_0$ a coefficient. Combining Eqs. (A4) and (A5) and imposing a periodic load function $P(t)$, we may integrate to determine the number of cycles to fracture

$$n_F = \gamma(fd/\upsilon_0)(Td^{3/2}/P_m)^N \quad , \tag{A6}$$

where $\gamma$ is a dimensionless quantity

$$\gamma = \int_{c_0}^{c_*} \mathrm{d}(c/d)/[G(c/d)]^N \quad ,$$

with $c_0$ the initial crack size.

Equation (A6), while approximate, provides explicit dependence of the number of cycles on key variables, specifically plate thickness $d$ and contact load $P_m$. Note the absence of $r$, indicating that near-contact conditions are not critical in the ultimate failure condition.